

Radiative Neutralino Decay in Split Supersymmetry

Marco Aurelio Díaz, Boris Panes, and Pedro Urrejola

Departamento de Física, Universidad Católica de Chile,

Avenida Vicuña Mackenna 4860, Santiago, Chile

(Dated: November 9, 2018)

Radiative neutralino decay $\chi_2^0 \rightarrow \chi_1^0 \gamma$ is studied in a Split Supersymmetric scenario, and compared with mSUGRA and MSSM. This 1-loop process has a transition amplitude which is often quite small, but has the advantage of providing a very clear and distinct signature: electromagnetic radiation plus missing energy. In Split Supersymmetry this radiative decay is in direct competition with the tree-level three-body decay $\chi_2^0 \rightarrow \chi_1^0 f \bar{f}$, and we obtain large values for the branching ratio $B(\chi_2^0 \rightarrow \chi_1^0 \gamma)$ which can be close to unity in the region $M_2 \sim M_1$. Furthermore, the value for the radiative neutralino decay branching ratio has a strong dependence on the split supersymmetric scale \tilde{m} , which is otherwise very difficult to infer from experimental observables.

I. INTRODUCTION

Split Supersymmetry (SS) was introduced in order to avoid some of the most notorious inconveniences of the Minimal Supersymmetric Standard Model (MSSM), namely, the lack of an automatic mechanism to avoid large flavour changing neutral currents and CP violation, and fast proton decay [1]. The strategy is to consider all scalars, with the exception of one Standard Model (SM) like Higgs boson, with a very large mass of the order of \tilde{m} , using unification of gauge couplings and the lightest supersymmetric particle (LSP) as Dark Matter candidate, as the only guiding principles [2]. In addition, motivated by the Cosmological Constant fine tuning problem, the electroweak scale fine tuning is accepted as a property of nature to be explained later by other principles to be discovered.

In this SS scenario, the light supersymmetric Higgs boson will have SM-like couplings and will be difficult to differentiate the two models in the absence of other signals [3]. The Large Hadron Collider will shortly start accelerating protons, and the best chance in this case for the larger detectors ATLAS [4] and CMS [5] to detect supersymmetry is in the chargino and neutralino sector [6]. While the lightest neutralino is the LSP, which is stable and candidate to dark matter in this R-Parity conserving model, the heavier neutralinos will decay into it. In SS, χ_2^0 will not have the chance to decay via intermediate scalars, and it will do it via intermediate Z bosons, $\chi_2^0 \rightarrow \chi_1^0 Z^* \rightarrow \chi_1^0 f \bar{f}$. The other important decay mode is generated at one-loop, the radiative decay of the neutralino $\chi_2^0 \rightarrow \chi_1^0 \gamma$, where all virtual charged particles contribute inside the loop [7]. This decay mode is well studied in the MSSM, and despite being generated

at one-loop, it can lead to large branching ratios [8].

In this article we are interested in the one-loop two-body decay mode $\chi_2^0 \rightarrow \chi_1^0 \gamma$ in Split Supersymmetry, and its relative size with respect to the tree-level three-body decay mode $\chi_2^0 \rightarrow \chi_1^0 f \bar{f}$. We study the region of parameter space where the radiative decay is enhanced, showing it to coincide with a relatively wide strip around $M_2 \sim M_1$. The signal for the radiative decay, an energetic photon plus missing energy, is clean and experimentally attractive, as long as the photon does not become too soft due to lack of phase space. We show that in this strip of parameter space, where the photon is still easily detectable [4], a measurement of the two main branching ratios can give information on the supersymmetric scale \tilde{m} . This is not a small feature because it is very difficult to measure the split supersymmetric scale in these models.

II. SPLIT SUPERSYMMETRY

Above the scale \tilde{m} the supersymmetric lagrangian is governed by the following R-Parity conserving superpotential,

$$W_{MSSM} = -\lambda^u \hat{H}_u \hat{Q} \hat{U} + \lambda^d \hat{H}_d \hat{Q} \hat{D} + \lambda^e \hat{H}_d \hat{L} \hat{E} - \mu \hat{H}_u \hat{H}_d \quad (1)$$

where λ^u , λ^d , and λ^e are the Yukawa coupling 3×3 matrices, and μ is the Higgs supersymmetric mass parameter. From this superpotential we highlight the following terms in the MSSM lagrangian,

$$\begin{aligned} \mathcal{L}_{MSSM} = & -\frac{g^2}{8} (H_u^\dagger \sigma^a H_u + H_d^\dagger \sigma^a H_d)^2 - \frac{g'^2}{8} (H_u^\dagger H_u - H_d^\dagger H_d)^2 \\ & - (m_{H_u}^2 + \mu^2) H_u^\dagger H_u - (m_{H_d}^2 + \mu^2) H_d^\dagger H_d + m_{H_{ud}}^2 (H_u^T \epsilon H_u + h.c.) \\ & + \lambda_{ij}^u H_u^T \epsilon \bar{u}_i q_j - \lambda_{ij}^d H_d^T \epsilon \bar{d}_i q_j - \lambda_{ij}^e H_d^T \epsilon \bar{e}_i \ell_j \\ & - \frac{H_u^\dagger}{\sqrt{2}} (g \sigma^a \tilde{W}^a + g' \tilde{B}) \tilde{H}_u - \frac{H_d^\dagger}{\sqrt{2}} (g \sigma^a \tilde{W}^a + g' \tilde{B}) \tilde{H}_d + h.c. \end{aligned} \quad (2)$$

where $\epsilon = i\sigma_2$. This lagrangian is valid at the scale \tilde{m} and above. At \tilde{m} the Higgs potential is characterized by quadratic terms proportional to squared gauge coupling constants, $g(\tilde{m})$ and $g'(\tilde{m})$, plus three mass terms. The two Higgs eigenstates are found to be rotations of H_u and H_d by an angle β , the lightest one given by $H = -\cos \beta \epsilon H_d^* + \sin \beta H_u$. Also in the MSSM lagrangian we have the Yukawa interactions with couplings $\lambda_{ij}^u(\tilde{m})$, $\lambda_{ij}^d(\tilde{m})$, and $\lambda_{ij}^e(\tilde{m})$. Finally, we see that the higgsino-Higgs-gaugino vertex are proportional to the gauge couplings, as Higgs-Higgs-gauge boson couplings are, as dictated by supersymmetry.

The Split supersymmetric lagrangian, valid at the scale \tilde{m} and below, is given by, [2]

$$\begin{aligned} \mathcal{L}_{SS} = & m^2 H H^\dagger - \frac{\lambda}{2} (H^\dagger H)^2 - \left[h_{ij}^u \bar{q}_j u_i \epsilon H^* + h_{ij}^d \bar{q}_j d_i H + h_{ij}^e \bar{\ell}_j e_i H + \right. \\ & \left. + \frac{H^\dagger}{\sqrt{2}} (\tilde{g}_u \sigma^a \tilde{W}^a + \tilde{g}'_u \tilde{B}) \tilde{H}_u + \frac{H^T \epsilon}{\sqrt{2}} (-\tilde{g}_d \sigma^a \tilde{W}^a + \tilde{g}'_d \tilde{B}) \tilde{H}_d + h.c. \right] \end{aligned} \quad (3)$$

where the Higgs field H is the surviving Higgs doublet at low energies. The Higgs potential is defined by a mass term m^2 and a quartic self coupling λ . The electroweak symmetry breaking occurs since $m^2 > 0$, and the Higgs field acquires a vacuum expectation value v . The matching condition for the Higgs self interaction at the split supersymmetric scale \tilde{m} is

$$\lambda(\tilde{m}) = \frac{g^2(\tilde{m}) + g'^2(\tilde{m})}{4} \cos^2 2\beta, \quad (4)$$

and this coupling should be run down to the weak scale to find the correct electroweak symmetry breaking. The Yukawa couplings in the split supersymmetric model are called h_{ij}^u , h_{ij}^d , and h_{ij}^e , and at the scale \tilde{m} the corresponding matching condition are

$$h_{ij}^u(\tilde{m}) = \lambda_{ij}^u(\tilde{m}) \sin \beta, \quad h_{ij}^{e,d}(\tilde{m}) = \lambda_{ij}^{e,d}(\tilde{m}) \cos \beta. \quad (5)$$

Finally, we notice from the Split Supersymmetric lagrangian in eq. (3) the Higgs-gaugino-higgsino interactions, whose couplings have the following matching conditions with the analogous terms in the MSSM lagrangian of eq. (2),

$$\begin{aligned} \tilde{g}_u(\tilde{m}) &= g(\tilde{m}) \sin \beta, & \tilde{g}_d(\tilde{m}) &= g(\tilde{m}) \cos \beta, \\ \tilde{g}'_u(\tilde{m}) &= g'(\tilde{m}) \sin \beta, & \tilde{g}'_d(\tilde{m}) &= g'(\tilde{m}) \cos \beta, \end{aligned} \quad (6)$$

The renormalization group equations for these and other couplings can be found in ref. [2]. For illustration we show in Fig. 1 some of their behaviour. In Fig 1(a) we have the running of the gauge coupling constants in Split Supersymmetry, which unify at the GUT scale as in the MSSM. In the second frame Fig. 1(b) we plot the Higgs-gaugino-higgsino couplings as a function of $\tan \beta$ for $\tilde{m} = 10^{16}$ GeV. If $\tan \beta = 1$, neither the boundary condition nor the RGE differentiate between \tilde{g}_u and \tilde{g}_d or between \tilde{g}'_u and \tilde{g}'_d . A sharp splitting appears when $\tan \beta$ increases. The down couplings become smaller than 0.1 for $\tan \beta \gtrsim 10$, while the up couplings approach asymptotically a maximum as $\tan \beta$ increases. In Fig. 1(c) we plot the Higgs-gaugino-higgsino couplings as a function of the split supersymmetric scale \tilde{m} . In Fig. 1(d) we plot the Higgs-gaugino-higgsino couplings normalized by the gauge couplings evaluated at the weak scale as a function of the scale \tilde{m} . We choose the value $\tan \beta = 50$, and observe deviations up to $\pm 20\%$. Of course, if the split supersymmetric scale is taken equal to the weak scale, there is no deviation.

Now we introduce the following notation,

$$\tan \tilde{\beta} \equiv \left. \frac{\tilde{g}_u}{\tilde{g}_d} \right|_{m_W} \simeq \tan \beta \left[1 + \frac{\cos 2\beta}{64\pi^2} \left(7g^2(\tilde{m}) - 3g'^2(\tilde{m}) \right) \ln \left(\frac{\tilde{m}}{m_W} \right) \right] \quad (7)$$

$$\tan \tilde{\beta}' \equiv \left. \frac{\tilde{g}'_u}{\tilde{g}'_d} \right|_{m_W} \simeq \tan \beta \left[1 - \frac{\cos 2\beta}{64\pi^2} \left(9g^2(\tilde{m}) + 3g'^2(\tilde{m}) \right) \ln \left(\frac{\tilde{m}}{m_W} \right) \right] \quad (8)$$

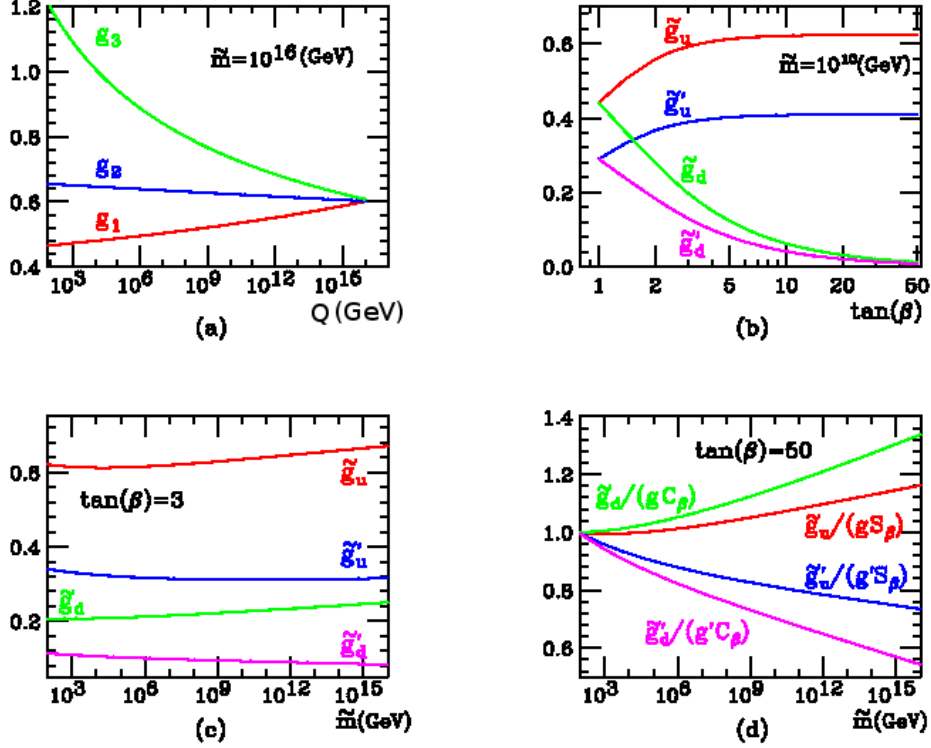


FIG. 1: (a) Gauge coupling unification is preserved in Split-SUSY. (b) Split-Susy couplings dependence on $\tan\beta$. (c) Split-Susy couplings evaluated at weak scale as function of \tilde{m} . (d) Split-Susy couplings normalized with gauge couplings evaluated at weak scale, for different values of \tilde{m} .

where it is understood that β is defined at the scale \tilde{m} , while $\tilde{\beta}$ and $\tilde{\beta}'$ are defined at the weak scale. The approximated expressions in eq. (8) is obtained from the corresponding RGE. These definitions together with,

$$\tilde{g}^2 \equiv \tilde{g}_u^2(m_W) + \tilde{g}_d^2(m_W), \quad \tilde{g}'^2 \equiv \tilde{g}'_u{}^2(m_W) + \tilde{g}'_d{}^2(m_W), \quad (9)$$

allow us to write the neutralino and chargino mass matrices in such a way it resembles those of the MSSM. The mixing angles $\tilde{\beta}$ and $\tilde{\beta}'$ are plotted in Fig. 2 as a function of \tilde{m} for $\tan\beta = 10, 50$. Of course, there is no difference between the three angles if $\tilde{m} = M_{weak}$.

With this notation, the neutralino mass matrix in Split Supersymmetric models has the following form,

$$\mathbf{M}_{\chi^0}^{SS} = \begin{bmatrix} M_1 & 0 & -\frac{1}{2}\tilde{g}'v\tilde{c}'_\beta & \frac{1}{2}\tilde{g}'v\tilde{s}'_\beta \\ 0 & M_2 & \frac{1}{2}\tilde{g}v\tilde{c}_\beta & -\frac{1}{2}\tilde{g}v\tilde{s}_\beta \\ -\frac{1}{2}\tilde{g}'v\tilde{c}'_\beta & \frac{1}{2}\tilde{g}v\tilde{c}_\beta & 0 & -\mu \\ \frac{1}{2}\tilde{g}'v\tilde{s}'_\beta & -\frac{1}{2}\tilde{g}v\tilde{s}_\beta & -\mu & 0 \end{bmatrix} \quad (10)$$

which is written in the usual basis $\psi^0 = (\tilde{B}, \tilde{W}^3, \tilde{H}_d^0, \tilde{H}_u^0)$. We have used the notation $\tilde{c}'_\beta \equiv \cos\tilde{\beta}'$,

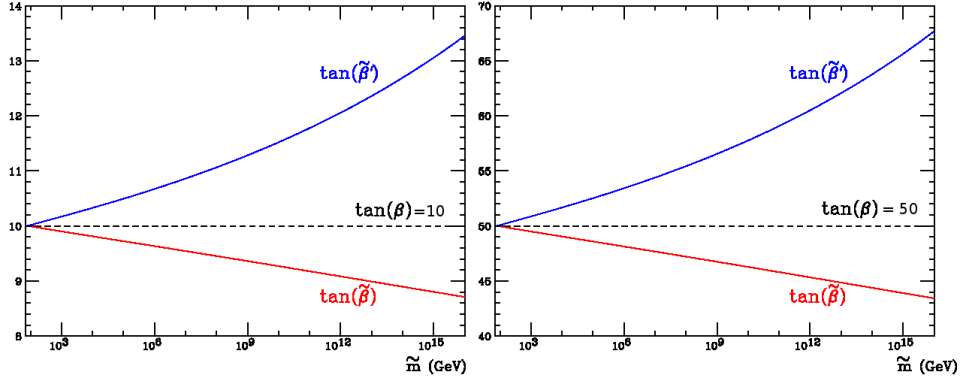


FIG. 2: Dependence of $\tan \tilde{\beta}$ and $\tan \tilde{\beta}'$ on the Split Supersymmetric scale, for different values of $\tan \beta$.

$\tilde{c}_\beta \equiv \cos \tilde{\beta}$, $\tilde{s}'_\beta \equiv \sin \tilde{\beta}'$, $\tilde{s}_\beta \equiv \sin \tilde{\beta}$. This mass matrix is diagonalized by the matrix N , such that $N^* \mathbf{M}_{\chi^0}^{SS} N^{-1} = (\mathbf{M}_{\chi^0}^{SS})_{diag}$, and the eigenvectors $\tilde{\chi}_i^0 = N_{ij} \psi_j^0$ are the neutralinos.

III. NEUTRALINO DECAYS IN MSUGRA AND SPLIT SUPERSYMMETRY

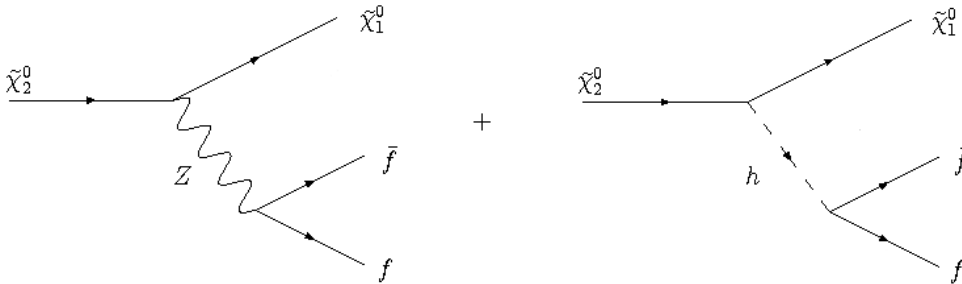


FIG. 3: Tree-level three body decay diagrams in Split-SUSY for the second lightest neutralino.

In Split Supersymmetry the three body decay modes of the second lightest neutralino receive contributions from intermediate gauge and light Higgs bosons, with negligible contribution from sfermions and heavy Higgs boson. These graphs are in Fig. 3, where the major contribution is from the Z -boson exchange, since the fermions in the final states have a very small mass. We calculate these decay rates integrating over the phase space with numerical techniques. We compare our calculations for the case of a small SS scale $\tilde{m} \sim 1$ TeV with results from the ISASUGRA code [9] with $m_0 \sim 1$ TeV. These are in agreement within small differences, the main of which is the distinctive running of Higgs-higgsino-gaugino couplings present in SS.

Our main interest in this article is the radiative decay of the second lightest neutralino into the LSP and a photon. This one-loop generated decay can shed light into the properties of heavy particles present in the

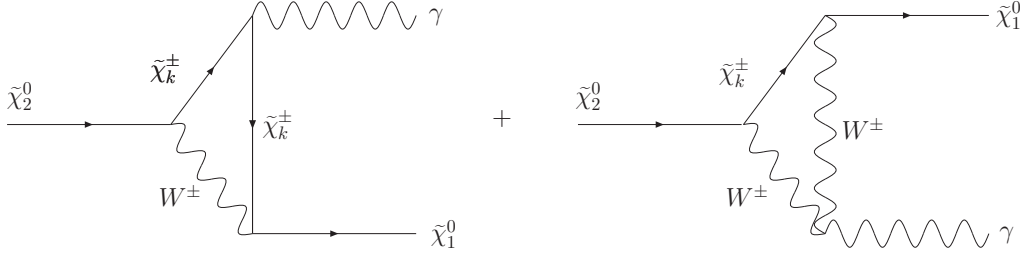


FIG. 4: Diagrams for the second lightest neutralino radiative decay into a photon and the lightest neutralino in Split-SUSY.

loop, charginos in the case of Split Supersymmetry. In addition, it is an experimentally interesting decay mode since it includes only a hard photon plus missing energy. Contributing loops in SS are displayed in Fig. 4. The loops include both charginos and W gauge bosons (charged Goldstone bosons are implicit). All other charged scalars which could contribute have a mass of the order of \tilde{m} and they are neglected. Of course, the effect of the heavy particles is felt via the RGE of the effective couplings below \tilde{m} . We calculate the integral over internal momenta analytically using dilogarithms [7].

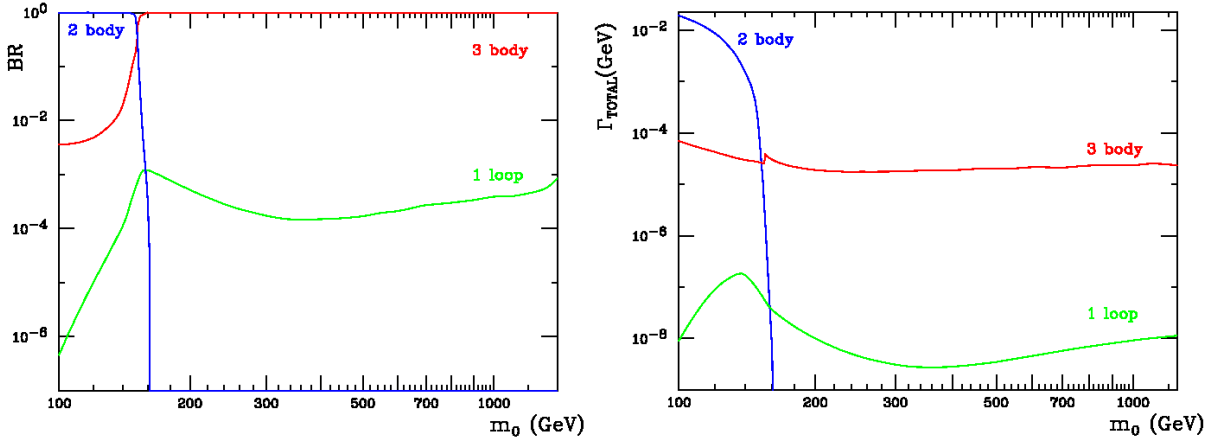


FIG. 5: Branching ratio and decay width for the different neutralino decay modes, in mSUGRA as a function of m_0 and around the SPS1a benchmark point.

In Fig. 5 we show the behaviour of the three main decay modes of the second lightest neutralino in mSUGRA: the tree-level two-body decay $\chi_2^0 \rightarrow \tilde{\ell}^\pm \ell^\mp$, the tree-level three-body decay $\chi_2^0 \rightarrow \chi_1^0 f \bar{f}$, and the one-loop two-body decay $\chi_2^0 \rightarrow \chi_1^0 \gamma$. We have Branching Ratios to the left and decay rates to the right, as a function of the universal scalar mass m_0 . The tree-level modes are calculated with the code ISASUGRA, while the one-loop mode with our code. The other parameters are taken as in benchmark SPS1a [10], which is given in Table I.

TABLE I: Input parameters for SPS1a mSUGRA benchmark point.

Parameter	Value	Units
m_0	100	GeV
$M_{1/2}$	250	GeV
A_0	100	GeV
$\tan \beta$	10	-
$\text{sign}(\mu)$	+1	-

TABLE II: Chargino and Neutralino masses for SPS1a.

Particle	Mass	Units
$\tilde{\chi}_1^0$	99	GeV
$\tilde{\chi}_2^0$	175	GeV
$\tilde{\chi}_3^0$	352	GeV
$\tilde{\chi}_4^0$	372	GeV
$\tilde{\chi}_1^+$	175	GeV
$\tilde{\chi}_2^+$	372	GeV

We can see that the one-loop decay rate $\Gamma(\chi_2^0 \rightarrow \chi_1^0 \gamma)$ has a maximum near $m_0 = 150$ GeV, decreasing for larger universal scalar mass. At values above $m_0 = 1$ TeV the mSUGRA result differs between 3-20% from our own SS result, calculated with values $\tilde{m} \gtrsim 1$ TeV. Of course, it is expected that mSUGRA results approach the SS result for large m_0 , since at large values of the universal scalar mass the triangular contributions from heavy scalar particles diminish. In SS the effect of these heavy particles appear through the RGE of the different couplings, but small differences remain between the two approaches because the running couplings include leading logarithm effects from all loops. We remind the reader that these RGE effects in SS do not spoil the unification of gauge coupling constants, as stressed in ref. [2] and illustrated in Fig. 1. The branching ratio $B(\chi_2^0 \rightarrow \chi_1^0 \gamma)$ remains between 10^{-3} and 10^{-4} for this mSUGRA scenario. In Table II we show the neutralino and chargino masses for $m_0 = 100$ GeV, with masses only slightly increasing (one or two GeV) for larger scalar mass, calculated using SUSPECT [11].

We compare in Fig. 5 the one-loop generated decay mode $\chi_2^0 \rightarrow \chi_1^0 \gamma$, with the tree-level decay modes. We define the tree-level two-body decay $\chi_2^0 \rightarrow \tilde{\ell}^\pm \ell^\mp$ as the sum of the three leptonic decays

TABLE III: Slepton and squark masses for SPS1a.

Particle	Mass	Units
$\tilde{e}_R, \tilde{\mu}_R$	145	GeV
$\tilde{e}_L, \tilde{\mu}_L$	204	GeV
$\tilde{\tau}_1$	136	GeV
$\tilde{\tau}_2$	208	GeV
\tilde{t}_1	375	GeV
\tilde{b}_1	491	GeV

TABLE IV: Input parameters for Split Supersymmetry benchmark point.

Parameter	Value	Units
M_1	102	GeV
M_2	192	GeV
M_3	587	GeV
μ	357	GeV
$\tan \beta$	10	-

$\chi_2^0 \rightarrow \tilde{e}e, \tilde{\mu}\mu, \tilde{\tau}\tau$ which occurs for values $m_0 \lesssim 160$ GeV, where the sleptons have a mass smaller than $m_{\chi_2^0}$. In this region, this decay mode dominates with a branching ratio near unity. We also have the tree-level three-body decay $\chi_2^0 \rightarrow \chi_1^0 f \bar{f}$, where we sum over all possible fermions. Above $m_0 \sim 160$ GeV the off-shell intermediate particles which contribute are the Z gauge boson and the squarks or sleptons, depending whether the final state fermion is a quark or a lepton. In this region the $B(\chi_2^0 \rightarrow \chi_1^0 f \bar{f})$ is near unity. Below $m_0 \sim 160$ GeV the contribution from the intermediate light on-shell sfermion is removed, and $B(\chi_2^0 \rightarrow \chi_1^0 f \bar{f})$ drops to a value between 10^{-3} and 10^{-2} . In Table III we show the slepton and the lightest squark masses for the SPS1a scenario using SUSPECT. For larger m_0 these masses grow up sharply, with right selectron and smuon becoming on-shell if $m_0 \lesssim 150$ GeV and similarly for the lightest stau if $m_0 \lesssim 155$ GeV. Both thresholds are fused into one in Fig. 5 because of the low resolution used in the graph.

In Fig. 6 we show the tree-level three-body decay $\chi_2^0 \rightarrow \chi_1^0 f \bar{f}$ and the one-loop two-body decay $\chi_2^0 \rightarrow \chi_1^0 \gamma$ in Split Supersymmetry, as a function of the wino mass M_2 , both calculated with our own code. We choose as SS benchmark point the one given in Table IV, whose soft gaugino and higgsino mass values

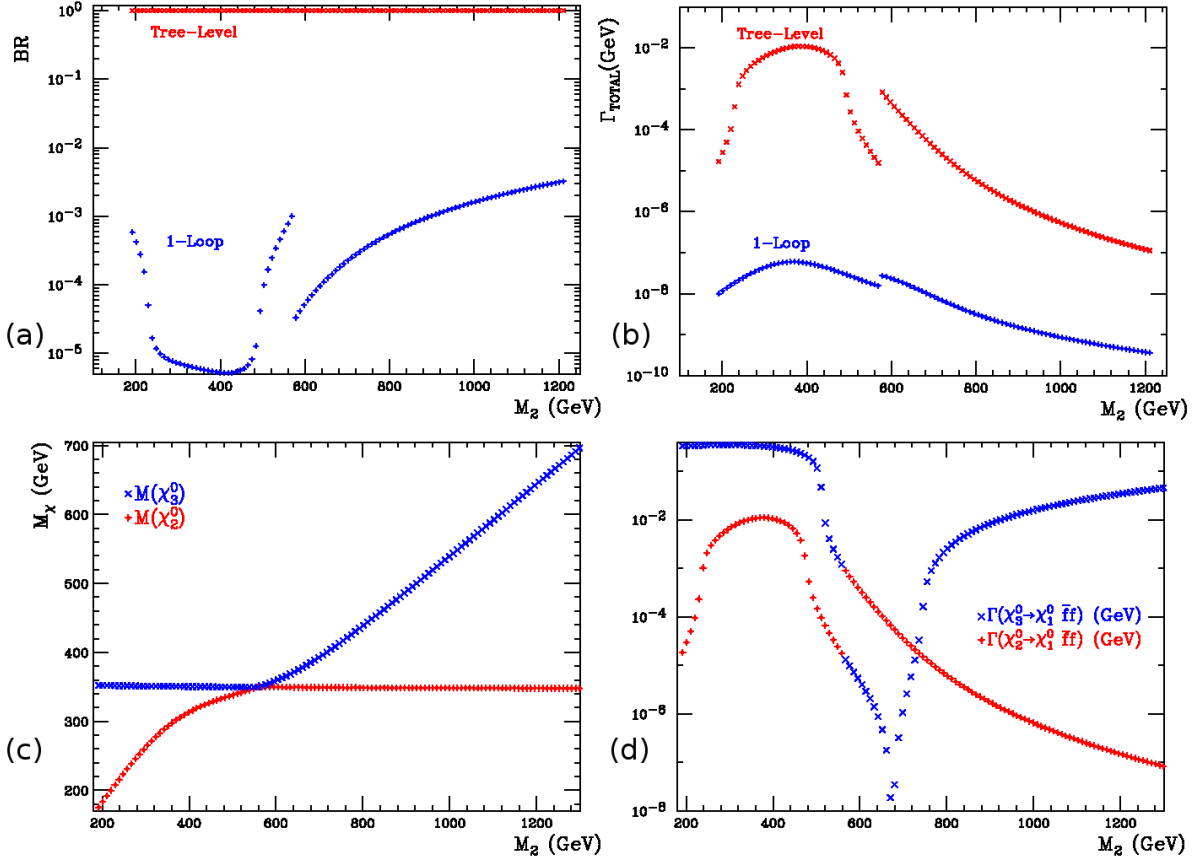


FIG. 6: Branching ratio (a) and decay width (b) for $\tilde{\chi}_2^0$ decay modes in SS as a function of M_2 . In (c) we see the mass eigenvalues crossing between the second and third neutralinos, which cause the discontinuous behaviour of the branching ratio and decay width (d).

coincide with the low energy soft masses from SPS1a. When varying the wino mass M_2 in Fig. 6, we vary also the bino mass M_1 keeping constant the M_2/M_1 ratio as in our SS benchmark scenario. In frame (a) we have the branching ratios, where tree-level three-body decay dominates over the one-loop decay $\chi_2^0 \rightarrow \chi_1^0 \gamma$ with a BR near unity. Since we work in SS, the $\chi_2^0 \rightarrow \chi_1^0 f \bar{f}$ mode is mediated only by an intermediate Z gauge boson. Similarly, the $\chi_2^0 \rightarrow \chi_1^0 \gamma$ decay is generated only by quantum corrections with W gauge bosons and charginos inside the loop.

In frame (b) we plot the decay rates for these two modes. The discontinuity on both decay rates occur near $M_2 \sim 560$ GeV and corresponds to an eigenvalue crossing. In frame (c) we see this eigenvalue crossing, with a $\tilde{\chi}_3^0$ higgsino type and $\tilde{\chi}_2^0$ gaugino type for $M_2 \lesssim 560$, while the opposite occurs for $M_2 \gtrsim 560$. The effect of the crossing can be seen very clearly in frame (d) where we have the three-body decays for both neutralinos $\tilde{\chi}_2^0$ and $\tilde{\chi}_3^0$.

IV. HIGH RADIATIVE NEUTRALINO DECAY BRANCHING RATIO

In this chapter we analyze with more detail the radiative decay for the second lightest neutralino, and look for conditions for an enhanced $B(\chi_2^0 \rightarrow \chi_1^0 \gamma)$ in Split Supersymmetry. In Fig. 7a we show with a

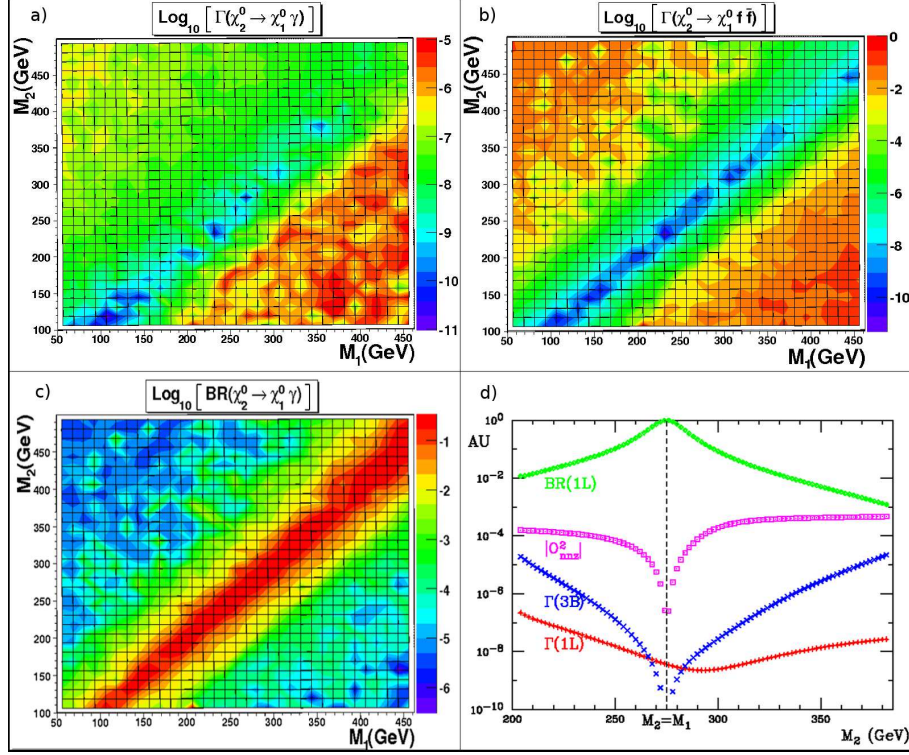


FIG. 7: (a) Radiative decay width, (b) 3-Body decay width, and (c) Branching ratio for the radiative mode in M_1 - M_2 plane in Split Supersymmetry. In (d) we have different curves as a function of M_2 showing the special behaviour at $M_1 = M_2$.

color code the logarithmic values for the decay rate $\Gamma(\chi_2^0 \rightarrow \chi_1^0 \gamma)$ in the gaugino mass plane M_1 - M_2 , with Γ measured in GeV. We show gaugino masses smaller than 500 GeV, and vary randomly the values for μ and $\tan \beta$. The largest values for the decay rate occur for $M_1 > M_2$, reaching typically up to 10^{-5} GeV. In the opposite case, when $M_1 < M_2$, the decay ratio varies typically between 10^{-7} and 10^{-8} GeV. There is a narrow fissure around $M_1 \sim M_2$ where the decay rate drops to values between 10^{-10} and 10^{-11} GeV. The fissure is not exactly at the bisector but somewhat deviated to the $M_1 > M_2$ side of the quadrant. In this fissure $\Delta m_\chi \equiv m_{\chi_2^0} - m_{\chi_1^0}$ is minimum, and the drop of the decay rate is a kinematical suppression.

In Fig. 7b we have a similar plot for the decay rate $\Gamma(\chi_2^0 \rightarrow \chi_1^0 f \bar{f})$, which is much larger than the previous case. This decay rate is more symmetrical with respect to the bisector, with decay rates reaching maximum values between 10^{-2} and 1 GeV, and a deep fissure at $M_1 \sim M_2$ going all the way down to 10^{-11} GeV or smaller. The fissure is situated over the bisector, and it is due to a zero in the neutralino-neutralino- Z

coupling, *i.e.* a dynamical suppression.

The branching ratio for the radiative decay $B(\chi_2^0 \rightarrow \chi_1^0 \gamma)$ is shown in Fig. 7c. We see that the second lightest neutralino one-loop generated decay $\chi_2^0 \rightarrow \chi_1^0 \gamma$ can dominate in a wide zone near the bisector $M_1 \sim M_2$. The reason for this possibility is that both decay rates decrease sharply in parallel fractures but slightly displaced. One of the fractures due to a zero in the $\chi^0 \chi^0 Z$ coupling (dynamical), and the other due to an eigenvalue degeneracy (kinematical). This is confirmed in Fig. 7d, where we show both decay rates, the radiative decay branching ratio, and the $\chi^0 \chi^0 Z$ coupling as a function of M_2 , with constant values for $M_1 = 275$ GeV, $\mu = 400$ GeV, $\tan \beta = 10$, and $\tilde{m} = 10^4$ GeV. We see that the zero for $\Gamma(\chi_2^0 \rightarrow \chi_1^0 f \bar{f})$ coincides with the zero for $\chi^0 \chi^0 Z$ coupling at $M_1 = M_2$, and that the minimum for $\Gamma(\chi_2^0 \rightarrow \chi_1^0 \gamma)$ coincides with the point where $m_{\chi_2^0} - m_{\chi_1^0}$ is minimum, at $M_2 \gtrsim M_1$.

In order to better understand the above result, it is instructive to see the neutralino mass matrix in the basis $[-i\tilde{\gamma}, -i\tilde{Z}, \tilde{H}_1, \tilde{H}_2]$, where

$$\begin{bmatrix} \tilde{\gamma} \\ \tilde{Z} \end{bmatrix} = \begin{bmatrix} c_W & s_W \\ -s_W & c_W \end{bmatrix} \begin{bmatrix} \tilde{B} \\ \tilde{W} \end{bmatrix}, \quad \begin{bmatrix} \tilde{H}_1 \\ \tilde{H}_2 \end{bmatrix} = \begin{bmatrix} c_\beta & -s_\beta \\ s_\beta & c_\beta \end{bmatrix} \begin{bmatrix} \tilde{H}_d \\ \tilde{H}_u \end{bmatrix}. \quad (11)$$

In this basis the mass matrix in eq. (10) looks as follows,

$$\mathbf{M}_{\chi^0} = \begin{bmatrix} \mathbf{M}_{\chi^0}^{gg} & \mathbf{M}_{\chi^0}^{gh} \\ \mathbf{M}_{\chi^0}^{hg} & \mathbf{M}_{\chi^0}^{hh} \end{bmatrix} \quad (12)$$

with $\mathbf{M}_{\chi^0}^{gh} = (\mathbf{M}_{\chi^0}^{hg})^T$. The different submatrices are equal to,

$$\begin{aligned} \mathbf{M}_{\chi^0}^{gg} &= \begin{bmatrix} M_1 c_W^2 + M_2 s_W^2 & (M_2 - M_1) s_W c_W \\ (M_2 - M_1) s_W c_W & M_1 s_W^2 + M_2 c_W^2 \end{bmatrix} \\ \mathbf{M}_{\chi^0}^{hh} &= \begin{bmatrix} \mu s_{2\beta} & -\mu c_{2\beta} \\ -\mu c_{2\beta} & -\mu s_{2\beta} \end{bmatrix} \end{aligned} \quad (13)$$

for the blocks in the diagonal, and

$$\mathbf{M}_{\chi^0}^{gh} = \frac{v}{2} \begin{bmatrix} c_\beta(\tilde{g}_d s_W - \tilde{g}'_d c_W) + s_\beta(\tilde{g}_u s_W - \tilde{g}'_u c_W) & s_\beta(\tilde{g}_d s_W - \tilde{g}'_d c_W) - c_\beta(\tilde{g}_u s_W - \tilde{g}'_u c_W) \\ c_W(c_\beta \tilde{g}_d + s_\beta \tilde{g}_u) + s_W(c_\beta \tilde{g}'_d + s_\beta \tilde{g}'_u) & c_W(s_\beta \tilde{g}_d - c_\beta \tilde{g}_u) + s_W(s_\beta \tilde{g}'_d - c_\beta \tilde{g}'_u) \end{bmatrix} \quad (14)$$

for the off diagonal block. This neutralino mass matrix reduces to its analogous expression in the MSSM if we neglect the running from \tilde{m} and the weak scale:

$$\mathbf{M}_{\chi^0}^{gh} \longrightarrow \frac{v}{2} \begin{bmatrix} 0 & 0 \\ g/c_W & 0 \end{bmatrix} \quad \text{as} \quad \tilde{m} \longrightarrow m_{weak}. \quad (15)$$

In the MSSM case, the direct mixing between photino and higgsinos vanishes, but a direct coupling between zino and one of the higgsinos remains. This implies that in general the lightest neutralino has a non vanishing component of higgsino, which in turn translates into a non vanishing $\chi^0\chi^0Z$ coupling. In this way, the photino will decouple from higgsinos in the region $M_1 \sim M_2$, as seen from eq. (13), and the decay rate $\Gamma(\chi_2^0 \rightarrow \chi_1^0 f \bar{f})$ vanishes also, making the decay $\chi_2^0 \rightarrow \chi_1^0 \gamma$ the dominant one. In SS the mechanism is similar, but modified by RGE effects.

As we mentioned, in the dynamical suppression region where $M_1 \sim M_2$ the decay mode $\Gamma(\chi_2^0 \rightarrow \chi_1^0 f \bar{f})$ is suppressed because the Z coupling to the photino is absent, thus, when the LSP is nearly photino, the $Z\chi_1^0\chi_2^0$ coupling is nearly zero. In the MSSM this region does not exactly coincides with the kinematical suppression region where $m_{\chi_1^0} \sim m_{\chi_2^0}$ due to the remanent higgsino-gaugino mixing seen in eq. (15). In this case, phase space is small, and χ_2^0 may be forced to decay into light mesons. The situation is similar

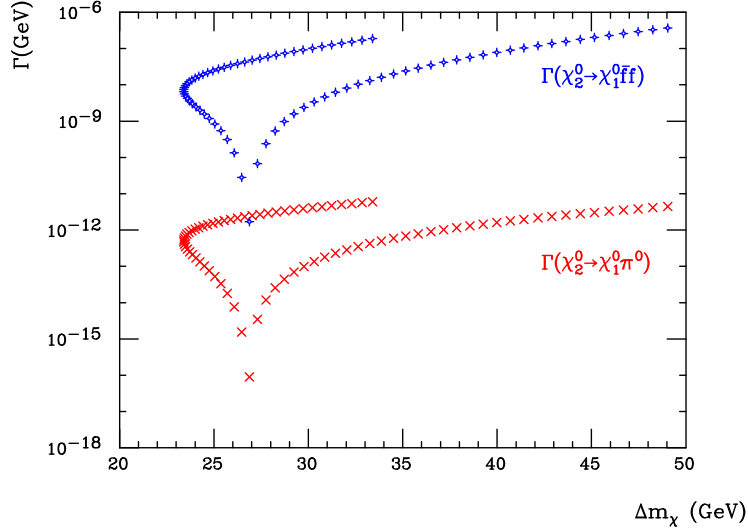


FIG. 8: Decay rate for $\chi_2^0 \rightarrow \chi_1^0 \pi^0$ in comparison to the decay rate for $\chi_2^0 \rightarrow \chi_1^0 f \bar{f}$, as a function of the mass difference $\Delta m_\chi = m_{\chi_2} - m_{\chi_1}$.

in Split Supersymmetry where the difference lies in the fact that in SS RGE effects separate further the regions where $Z\chi_1^0\chi_2^0$ coupling and Δm_χ vanish, as indicated by the higgsino-gaugino mixing in eq. (14). In Fig. 8 we have plotted the decay rate $\Gamma(\chi_2^0 \rightarrow \chi_1^0 f \bar{f})$ and the (included in the former) decay rate $\Gamma(\chi_2^0 \rightarrow \chi_1^0 \pi^0)$ as a function of Δm_χ . The independent variable we are varying is M_2 , exactly as in Fig. 7d. Both decay rates vanish at the point where the $Z\chi_1^0\chi_2^0$ coupling is null, but at that point Δm_χ is not zero. Indeed, in Fig. (8) we have $\Delta m_\chi = 26.8$ GeV for $\tilde{m} = 10$ TeV, while RGE effects changes it to $\Delta m_\chi = 29.2$ GeV for $\tilde{m} = M_{GUT}$. Therefore, the photon in the decay $\chi_2^0 \rightarrow \chi_1^0 \gamma$ will have enough energy to be easily detected. Note that the two branches in each decay are defined by the sign of $M_2 - M_1$.

As we discussed, in Split Supersymmetry the mechanism is analogous to the MSSM, but the details are modified by the Renormalization Group Equations effects. Indeed, the remaining higgsino component of the lightest neutralino in the case $M_1 = M_2$ is controlled by the SS scale \tilde{m} via the RGE effects on the different couplings. This can be seen in Fig. 9 where we have the χ_2^0 branching ratios dependence on $\tan\beta$

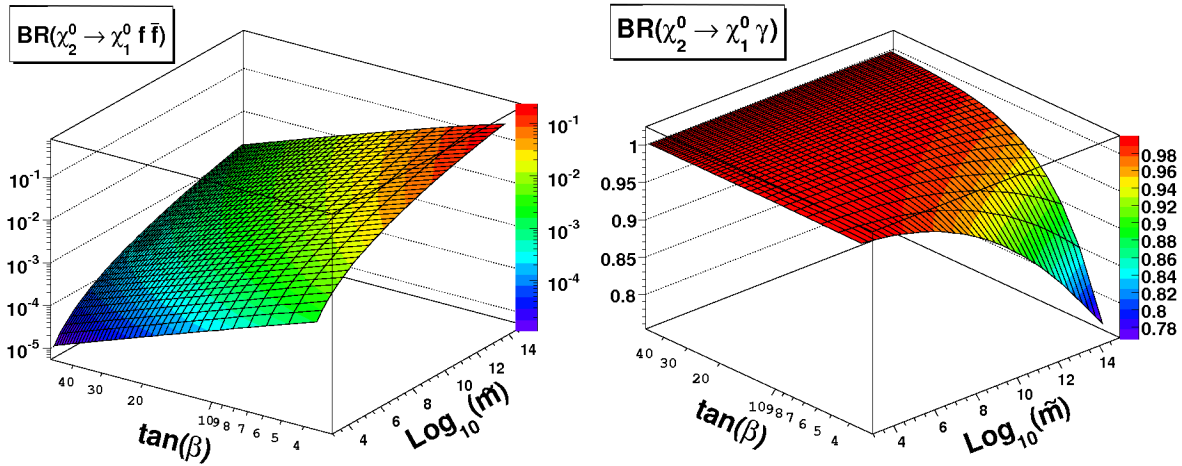


FIG. 9: χ_2^0 decay modes as a function of the Split Susy scale \tilde{m} and $\tan\beta$ for the scenario where $M_1 = M_2$.

and the SS scale \tilde{m} , with $\mu = 400$ GeV and $M_1 = M_2 = 275$ GeV. The dependence on $\tan\beta$ is relatively mild, as it is the dependence on \tilde{m} . But in comparison to other observables, the dependence on the SS scale is very important, because in this scenario a measurement of the χ_2^0 branching ratios could yield valuable information on the SS scale, otherwise difficult to extract from experiments. In the right frame we see that $B(\chi_2^0 \rightarrow \chi_1^0 \gamma)$ dominates over a large region, with a small decrease at small $\tan\beta$ and large \tilde{m} . In the left frame we have $B(\chi_2^0 \rightarrow \chi_1^0 f \bar{f})$, with values that go from 10^{-5} up to 0.2. Clearly, a measurement of the branching ratio can give valuable information on the split supersymmetric scale.

V. CONCLUSION

We have calculated the decay rates and branching ratios of the second lightest neutralino in Split Supersymmetry, and concentrate in the radiative decay $\chi_2^0 \rightarrow \chi_1^0 \gamma$. We compared our results with mSUGRA, finding agreement when the scalar mass parameter is very large, $m_0 \sim 1$ TeV, where $B(\chi_2^0 \rightarrow \chi_1^0 \gamma) \sim 10^{-3}$. Small differences remain due to RGE effects, which increase with larger split supersymmetric scale \tilde{m} . For larger values of m_0 comparison is not possible since large squark masses in quantum corrections destabilize the EWSB in direct mSUGRA calculations.

In general models, the possibility that $m_{\chi_2^0}$ is not much different than the mass of the LSP is experimentally challenging. This is because the decay products that can be detected, photons in the case of $\chi_2^0 \rightarrow \chi_1^0 \gamma$ and fermions in the case of $\chi_2^0 \rightarrow \chi_1^0 f \bar{f}$, are soft and specialized analysis have to be done with the data. Nevertheless, in our model the radiative decay dominates in a region where Δm_χ is large enough to produce an energetic photon. We focus on the region $M_1 \sim M_2$, where this possibility is realized and show that the decay $\chi_2^0 \rightarrow \chi_1^0 \gamma$ is dominant in a wide band around the bisector $M_1 = M_2$. Furthermore, in this region a measurement of the branching ratios $B(\chi_2^0 \rightarrow \chi_1^0 \gamma)$ and $B(\chi_2^0 \rightarrow \chi_1^0 f \bar{f})$ can give information on the value of the split supersymmetric scale \tilde{m} .

Acknowledgments

We are indebted to Dr. Pavel Fileviez-Pérez for his insight in the early stages of this work. We are thankful to Dr. Benjamin Koch for useful comments. This work was partly funded by Conicyt and Banco Mundial grant “Anillo Centro de Estudios Subatómicos”, by Conicyt’s “Programa de Becas de Doctorado”, and by VRAID-PUC fellowships.

-
- [1] N. Arkani-Hamed and S. Dimopoulos, *JHEP* **0506**, 073 (2005) [arXiv:hep-th/0405159].
- [2] G. F. Giudice and A. Romanino, “Split supersymmetry”, *Nucl. Phys. B* **699**, 65 (2004) [Erratum-ibid. *B* **706**, 65 (2005)] [arXiv:hep-ph/0406088].
- [3] F. Wang, W. Wang, F. q. Xu, J. M. Yang and H. Zhang, *Eur. Phys. J. C* **51**, 713 (2007) [arXiv:hep-ph/0612273]; S. K. Gupta, B. Mukhopadhyaya and S. K. Rai, *Phys. Rev. D* **73**, 075006 (2006) [arXiv:hep-ph/0510306]; M. A. Diaz and P. Fileviez Perez, *J. Phys. G* **31**, 563 (2005) [arXiv:hep-ph/0412066]; K. Cheung and J. Song, *Phys. Rev. D* **72**, 055019 (2005) [arXiv:hep-ph/0507113].
- [4] G. Aad *et al.* [The ATLAS Collaboration], “Expected Performance of the ATLAS Experiment - Detector, Trigger and Physics,” arXiv:0901.0512 [hep-ex].
- [5] R. Adolphi *et al.* [CMS Collaboration], “The CMS experiment at the CERN LHC,” *JINST* **0803** (2008) S08004 [JINST **3** (2008) S08004].
- [6] G. Polesello, *J. Phys. G* **30** (2004) 1185.
- [7] H. E. Haber and D. Wyler, *Nucl. Phys. B* **323**, 267 (1989).
- [8] S. Ambrosanio and B. Mele, *Phys. Rev. D* **55**, 1399 (1997) [Erratum-ibid. *D* **56**, 3157 (1997)] [arXiv:hep-ph/9609212].
- [9] F. E. Paige, S. D. Protopopescu, H. Baer and X. Tata, “ISAJET 7.37: A Monte Carlo event generator for p p, anti-p p, and e+ e- reactions,” arXiv:hep-ph/9804321.
- [10] N. Ghodbane and H. U. Martyn, “Compilation of SUSY particle spectra from Snowmass 2001 benchmark models,” in *Proc. of the APS/DPF/DPB Summer Study on the Future of Particle Physics (Snowmass 2001)* ed. N. Graf, arXiv:hep-ph/0201233.
- [11] A. Djouadi, J. L. Kneur and G. Moultaka, “SuSpect: A Fortran code for the supersymmetric and Higgs particle spectrum in the MSSM,” *Comput. Phys. Commun.* **176**, 426 (2007) [arXiv:hep-ph/0211331].